2024 IEEE International Conference on Robotics and Automation (ICRA 2024)
May 13-17, 2024. Yokohama, Japan

Research on bionic foldable wing for flapping wing micro air vehicle

Shengjie Xiao[1], Kai Hu[1], Yuhong Sun[1], Yun Wang[1], Bo Qin[1], Huichao Deng[1,*], Xuan Wu[2], and Xilun Ding[1], *Member IEEE*

***Abstract*— This paper presents a bionic foldable wing that imitates the hind wing of ladybirds. Based on the folding mechanism of the hind wing of ladybirds and the theory of origami, the motion model of the bionic foldable wing is established, yield the motion law of the crease angles and the variation relationship between the panels are obtained. Bionic foldable wings utilise shape memory alloy to drive wings to fold, and embedded torsion springs to release energy to realize the function of wing unfolding. In the experiments of the vehicle equipped with foldable wings, the lift and attitude torque of bionic foldable wings are measured by the F/T sensor. The experimental results indicated that its aerodynamic performance is basically close to that of our optimized non-foldable wings. Moreover, the vehicle with foldable wings has been able to overcome gravity to achieve flight, which provides a novel concept for the research on flapping wing.**

I. Introduction

Insects can utilise unsteady lift mechanisms to produce a higher aerodynamic force, which results in higher flight mobility. The key point is that insects have precise and lightweight wings that can withstand high-frequency vibrations and generate high aerodynamic forces. Ladybirds, members of the order Coleoptera, possess both front (Coleoptera) and hind wings. The hind wings of ladybirds have a special efficient and complex folding method that effectively utilises the flexibility and elasticity of the mechanism to achieve complex transformation. As a new type of vehicle, flapping wing micro air vehicles (FWMAVs) are different from rotor and fixed-wing vehicles, and they have significant advantages in term of energy efficiency and bionic shape, including hovering flight capabilities. FWMAVs with foldable wings can reduce their size, increase concealment and portability while performing tasks, and expand their mission spaces. Therefore, the design of bionic foldable wings have become a key issue in the research on FWMAVs. [1, 2].

Muhammad et al. [3, 4] developed a four-layer separated bionic foldable wing model based on the four plate theory and the hind wing of xylotrupes dichotomus. It used the characteristics of the shape memory alloy (SMA) wire to perform the folding motion. Truong et al. [5] designed a bionic foldable wing based on four-bar mechanism. Stowers et al. [6] proposed a new mechanism for passive wing deformation, inspired by the wings of bats and birds. This flapping motion produces centrifugal acceleration on the hand wing, forcing it to expand passively. The bat-like FWMAV "Bat Bot2" designed by Seth et al. [7] can realise the folding function of its wings. The wing frame was composed of a four-bar mechanism driven by a ball-screw mechanism, and the wing was composed of carbon fibre and a silicone film. Kova et al. [8] uses carbon fibre rods to build the structural skeleton and the wings are covered with miral foil, which uses an SMA-locking mechanism to unfold and retract its wings. He et al. [9] proposed a design scheme for a flapping-wing vehicle imitating bats based on the bat flight mode. By driving with a single actuator, coupled and coordinated motions of flapping and folding were achieved, and the power coefficient of the system was improved.

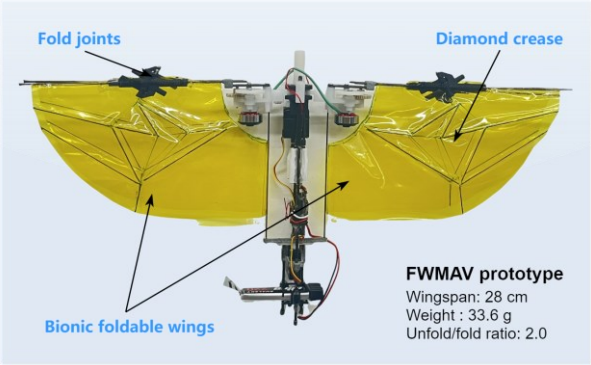

Fig. 1. FWMAV with bionic foldable wings.

Wu et al. [10] used the hind wings of a scarab as a bionic object, analysed the kinematics of its unfolding and retracting processes, and proposed an unfolding and retracting scheme for foldable wings based on hydraulic control. The structural skeleton of this wing was made of ABS plastic, and the liquid channel was arranged in a vein rod. The joints were connected using ABS plastic pipes, and the temperature of the alcohol liquid was controlled using a silicone heating plate at the root of the wings. Phan et al. [11, 12] developed an insect-like vehicle with passive foldable wings. In the flight process, the wings flap normally; once external interference occurs on the wings, the passive joints of the wings can be folded and deformed, and the flight attitude can be adjusted quickly to realise the anti-interference flight of the vehicle. Sangmin et al.[13] have developed a multimodal robot based on ladybird self-locking joints and origami mechanisms. In previous research on foldable wings, the focus was mainly on driving methods, joint design, and new materials to make the wing folding ratio as close as possible to biological parameters; however, there is a lack of research on the folding mechanism and flight performance of bionic foldable wings.

This research was supported by the National Natural Science Foundation of China under Grant No. 51975023 & 52322501. This work was supported in part by the National Natural Science Foundation of China under Grant No. U22B2040.

[1] Space Robot Laboratory, the School of Mechanical Engineering, Beihang University, Beijing 100191, China.

[2] Robotics Laboratory, China Nanhu Academy of Electronics and Information Technology, Jiaxing 314000, China.

*Corresponding author: Huichao Deng, denghuichao@buaa.edu.cn.

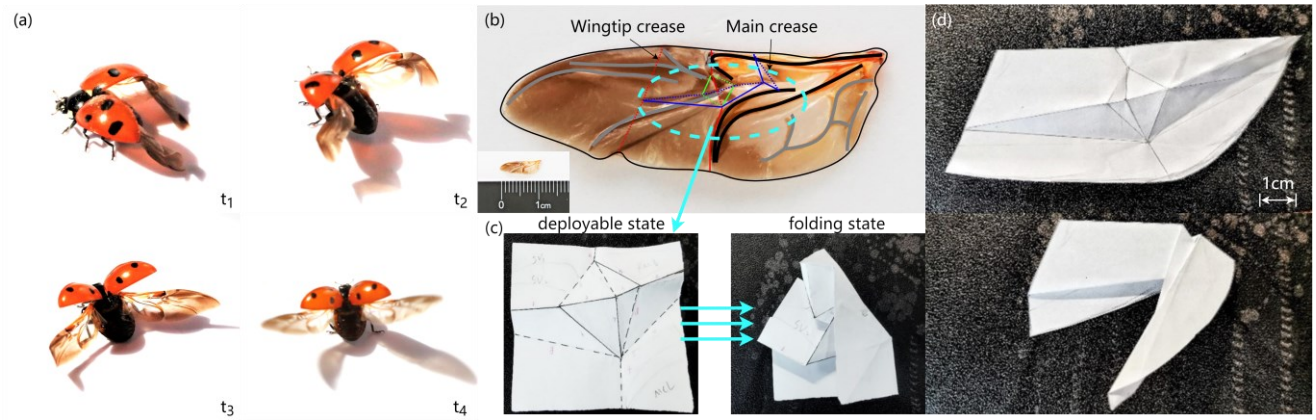

Fig. 2. Hind wings of ladybird with unfolding movements. (a) Unfolding process of hind wing. (b) Biological structure of hind wing of ladybird. (c) Origami mechanism based on main crease. (d) Origami experiment of bionic wing.

In this study, a FWMAV equipped with bionic foldable wings was devised, as shown in Fig.1. Considering ladybirds and their hind wings as bionic objects, we discuss the folding mechanism and motion mode of the hind wings of ladybirds. The adjacency matrix method was used to calculate the degrees of freedom of the folding mechanism, and a motion model based on the multi vertex origami mechanism was constructed; Subsequently, by using a combination of an SMA and torsion springs, a proportional amplification prototype of the folding wing was manufactured, achieving the folding and unfolding functions of the wing. Finally, flight testing of the vehicle equipped with bionic foldable wings was conducted [14,15]. This driving design solves the problem of balancing wing rigidity and flexibility and has excellent aerodynamic performance.

The remainder of this paper is organised as follows. Section 2 introduces the structure and folding mechanism of the hind wings of ladybirds. The folding motion of the hind wings of ladybirds is reproduced using origami. Section 3 shows the crease layout of bionic foldable wing, and analyse the folding mode and wing folding mechanism of the ladybird. In Section 4, the entire structure of the bionic foldable wing and aerodynamic force/torque experiments using the F/T sensor are explained. Finally, the conclusions and contributions of this study are summarised in Section 5.

II. Bio-inspiration

Achieving compatibility between the deformation instability required for storage and the strength stability required for flight is crucial for ladybird hind wings, and these two characteristics are usually compromised. The edge and ventral side of the hindwing vein and the characteristic shape of the vein, play important roles in wing folding. The process of unfolding the hind wings of a ladybird is shown in Fig. 2(a).

Fig. 2(b) shows the hind wing structure of a ladybird and a simplified wing vein diagram [16,17]. The base of the hind wing is supported by two thick veins, the middle elbow vein and the radial mid vein, and the middle and posterior segments of the wing are supported by other veins. The wing membrane crease is divided into transverse and longitudinal creases based on its distribution trend. Kazuya et al. [17] proposed the creases are distributed longitudinally, in which the solid line is raised, called the "peak", and the dotted line is concave, called the "valley". Red creases are transverse creases called the transverse main creases and lateral wing-tip creases. The two types of lines are connected by diamond crease patterns (green lines), the diamond-shaped creases was shown in Fig.2(c). These rhombic creases are rarely involved in the overall deformation of the hind wings. Researchers speculated that these additional folds on the ridge of the central crease line may be locking mechanisms that help avoid accidental deployment caused by wing elasticity [18,19]. Fig.2(d) show folding movements of the hind wings reproduced using origami with a folding ratio (unfolded wing area/folded wing area) of 1.9.

III. Kinematic Analysis

As shown in Fig. 3, the origami mechanism used in this study is a multi-vertex origami mechanism with five non-boundary vertices. We employed the adjacency matrix method to calculate the degrees of freedom of the folding mechanism [20]. Therefore, the coordinate transformation of these five vertices and the relationship between the common creases were analysed [21, 22]. $P_1, P_2, \ldots P_{10}$ on each panel of the mechanism are marked in the counterclockwise direction, and the crease is marked in the counterclockwise direction

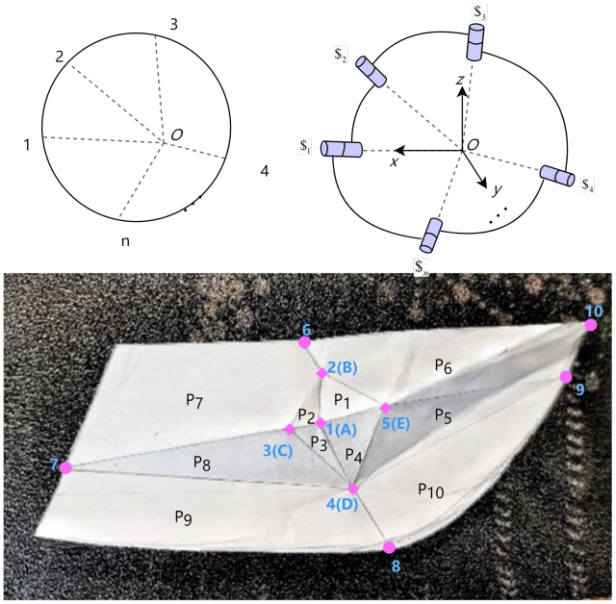

Fig. 3. Diagram of aerodynamic force/torque test system.

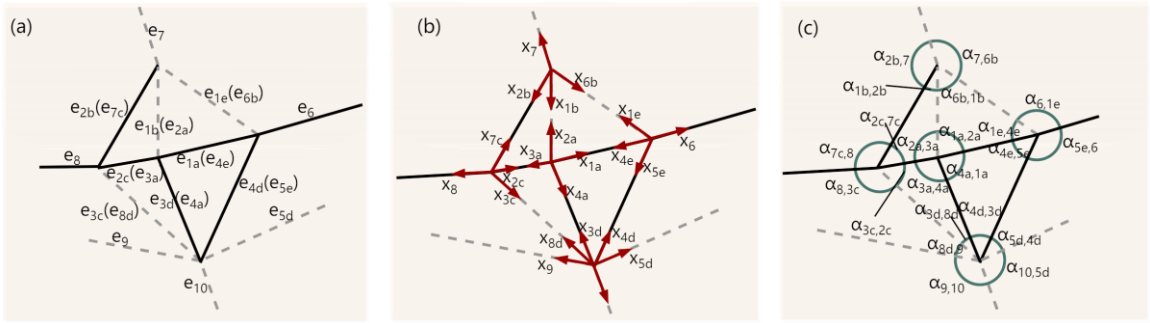

Fig. 4. Kinematic analysis of wing origami mechanism. (a) Multi vertex origami mechanism. (b) Coordinate system based on crease of the origami mechanism. (c) Crease angle of vertex.

according to the vertex in Fig. 4(a). Because the creases intersecting the non-boundary vertices have common creases and panels, to avoid overlapping, the common crease subscripts are labelled with vertex labels; for example, the crease between A and E is marked as e_{1a} and e_{4a}.

As shown in Fig. 4(b), a Cartesian coordinate system was established at the crease of the origami mechanism [23]. Take the crease intersecting A as an example, set the coordinate origin o_{1a} at vertex A, the x_{1a}-axis is along the direction of crease e_{1a} and points outward from the origin of the coordinate. The z_{1a} axis is perpendicular to P_1, the direction is from the origin of the coordinate to the direction of the panel depression when folding. Finally, the direction of y_{1a}-axis is determined by right-hand rule, that is, the coordinate system $o_{1a}x_{1a}y_{1a}z_{1a}$ is established at the crease. Similarly, cartesian coordinates of creases at B, C, D and E can be established respectively.

In Fig. 4(c), suppose the angle between the x_i-axis and the x_j-axis be $\alpha_{i,j}$, the direction from the x_i-axis counterclockwise to the x_j-axis. The angle between adjacent creases intersecting at the same point is constant; the corresponding $\alpha_{i,j}$ is also constant; and the angle between the z_i-axis and the z_j-axis is $\gamma_{i,j}$, which is the direction from the z_i-axis counterclockwise to the z_j-axis. If the dihedral angle between panels P_i and P_j is $\theta_{i,j}$.

$$\theta_{i,j} = \pi - \left|\gamma_{i,j}\right| \tag{1}$$

There are eight common creases in the origami mechanism, and the dihedral angles between the two common panels on both sides of each common crease are equal.

$$\begin{cases} \theta_{1a,2a} = \theta_{2b,1b} & \theta_{1b,6b} = \theta_{6e,1e} \\ \theta_{2a,3a} = \theta_{3c,2c} & \theta_{7b,2b} = \theta_{2c,7c} \\ \theta_{3a,4a} = \theta_{4d,3d} & \theta_{8,3c} = \theta_{3d,8d} \\ \theta_{4a,1a} = \theta_{1e,4e} & \theta_{5d,4d} = \theta_{4e,5e} \end{cases} \tag{2}$$

Only a rotational transformation exists between two adjacent coordinate systems, $o_ix_iy_iz_i$ and $o_jx_jy_jz_j$, whose origins coincide. First, $o_ix_iy_iz_i$ is rotated counterclockwise $\alpha_{i,j}$ degrees around the z_i-axis and then to $o_jx_jy_jz_j$ anticlockwise $\gamma_{i,j}$ degrees around the x_j-axis to get the transformation matrix ${}^j_iT$.

For the transformation between coordinate systems whose origins are not coincident, for example, there is a common crease $e_{2a}(e_{1b})$ between A and B vertices. Suppose $\overline{AB} = a$. In Fig. 4(b), the coordinate system $o_{2a}x_{2a}y_{2a}z_{2a}$ rotates $\alpha_{2a,1b}°$ counterclockwise around the z_{2a}-axis, then translates a along the negative direction of the x_{2a}-axis, and finally rotates $\gamma_{2a,1b}°$ counterclockwise around the x_{1b}-axis to obtain the coordinate system $o_{1b}x_{1b}y_{1b}z_{1b}$ and transformation matrix ${}^{2a}_{1b}T$.

$$\begin{aligned} {}^j_iT &= R(Z_i,\alpha_{i,j})R(X_i,\gamma_{i,j}) \\ &= \begin{bmatrix} \cos\alpha_{i,j} & -\sin\alpha_{i,j} & 0 & 0 \\ \sin\alpha_{i,j} & \cos\alpha_{i,j} & 0 & 0 \\ 0 & 0 & 1 & 0 \\ 0 & 0 & 0 & 1 \end{bmatrix} \begin{bmatrix} 1 & 0 & 0 & 0 \\ 0 & \cos\gamma_{i,j} & -\sin\gamma_{i,j} & 0 \\ 0 & \sin\gamma_{i,j} & \cos\gamma_{i,j} & 0 \\ 0 & 0 & 0 & 1 \end{bmatrix} \\ &= \begin{bmatrix} \cos\alpha_{i,j} & -\sin\alpha_{i,j}\cos\gamma_{i,j} & \sin\alpha_{i,j}\sin\gamma_{i,j} & 0 \\ \sin\alpha_{i,j} & \cos\alpha_{i,j}\cos\gamma_{i,j} & -\cos\alpha_{i,j}\sin\gamma_{i,j} & 0 \\ 0 & \sin\gamma_{i,j} & \cos\gamma_{i,j} & 0 \\ 0 & 0 & 0 & 1 \end{bmatrix} \end{aligned} \tag{3}$$

All coordinate systems whose coordinate origins coincide with a point form a closed-loop system. Therefore, the motion

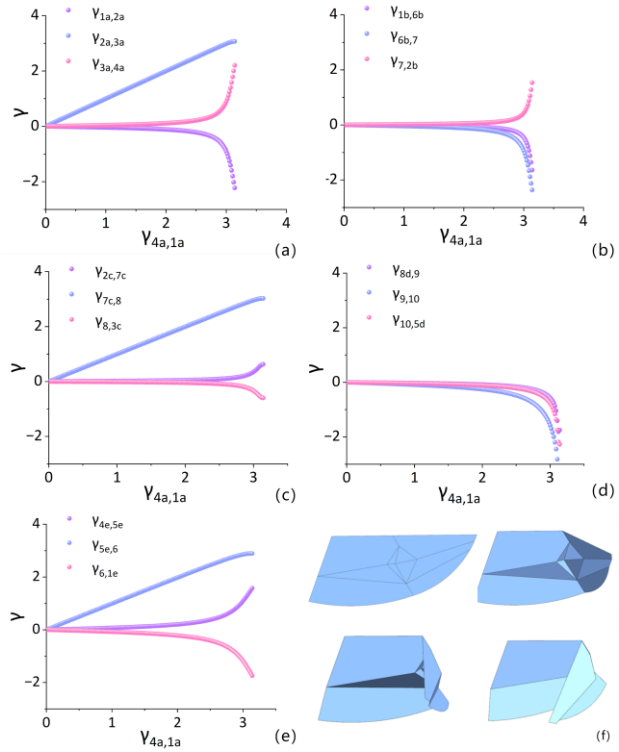

Fig. 5. Simulation of bionic foldable wing mechanism. (a) Crease angle at point A. (b) Crease angle at point B. (c) Crease angle at point C. (d) Crease angle at point D. (e) Crease angle at point E. (f) Folding process.

model of the origami mechanism can be determined as follows:

$$\begin{cases} I_A = {}^{2a}_{1a}T \cdot {}^{3a}_{2a}T \cdot {}^{4a}_{3a}T \cdot {}^{1a}_{4a}T \\ I_B = {}^{6b}_{1b}T \cdot {}^{7}_{6b}T \cdot {}^{2b}_{7}T \cdot {}^{1b}_{2b}T \\ I_C = {}^{7c}_{2c}T \cdot {}^{8}_{7c}T \cdot {}^{3c}_{8}T \cdot {}^{2c}_{3c}T \\ I_D = {}^{8d}_{3d}T \cdot {}^{9}_{8d}T \cdot {}^{10}_{9}T \cdot {}^{5d}_{10}T \cdot {}^{4d}_{5d}T \cdot {}^{3d}_{4d}T \\ I_E = {}^{4e}_{1e}T \cdot {}^{5e}_{4e}T \cdot {}^{6}_{5e}T \cdot {}^{1e}_{36}T \end{cases} \quad (4)$$

I_i is the identity matrix.

It can be observed from the above that the mechanism has one DOF; therefore, this research solves the motion model of the origami mechanism based on the method of deriving explicit expressions. Because e_{1a} and e_{3a} are mountain creases, the change direction of $\gamma_{4a,1a}$ and $\gamma_{2a,3a}$ during folding is the same, which is set as the positive direction. There is a common crease between vertex A and the other four non-boundary vertices in the origami mechanism, the change speed of input parameters $\gamma_{4a,1a}$ and $\gamma_{2a,3a}$ is the same, and the value range of angle is $[0, \pi]$. The curves of angle γ relative to the input angle $\gamma_{4a,1a}$ at the crease of each non-boundary vertex are shown in Fig. 5(a) ~ Fig.5(e).

The change speed of $\gamma_{7c,8}$ and $\gamma_{5e,6}$ relative to the input angle $\gamma_{4a,1a}$ is nearly uniform, and the change speed is similar to that of $\gamma_{2a,3a}$; this is because of the special folding mode of the folding mechanism, and the four creases are mountain creases. The four creases are located in the middle of the origami mechanism, and the head and tail are connected, which is close to a straight line. Thus, the changes in creases e_8, $e_{3a}(e_{2c})$ and e_6 relative to crease e_{1a} tend to be uniform. The folding curve of each crease angle is smooth and has no mutation, and the final state value γ is consistent with the actual folding situation, which indicates that the folding mechanism has no singularity in the folding process. As shown in Fig. 5, the motion of each vertex forms a closed loop. The dihedral angles of output creases e_{6b} and e_{1e} are equal; therefore, the origami mechanism is rigid and foldable. A diagram of the folding process of the origami mechanism is shown in Fig. 5(f).

IV. Experiments

A. Manufacture of foldable wing

The prototype of the bionic foldable wing was designed, as shown in Fig. 6(a). The wingspan of the foldable wing was 110 mm, chord length was 50 mm, slack angle to was 15 ~ 20° and the angle between the rod B and the driving crease was 59°, and folding ratio was 2.0. Carbon fibre rods (0.3 mm in diameter) were used as the bionic creases for the wing veins, and a carbon fibre rod with a diameter of 1 mm was used for the wing root. A polyimide film with a thickness of 25 μm was used as the wing membrane. The leading-edge rod was mainly used carbon fibre material. After assembly, the weight of a single foldable wing is 1.1 g.

The foldable mechanism is driven by SMA and torsion springs [24]. The red and blue coils represent the SMA and torsion spring, respectively. When the SMA spring is energised, the SMA is in an active state, and is twisted and compressed, accumulating energy, and the wing is in a folded state. Fig. 6(b) shows the folding process of the SMA spring after being energised. When the SMA is powered off, the energy stored by the torsion spring is released, the SMA spring is stretched, and the wings remain in an unfolded state.

B. Experimental test

The folding process is illustrated in Fig. 6(b). The entire

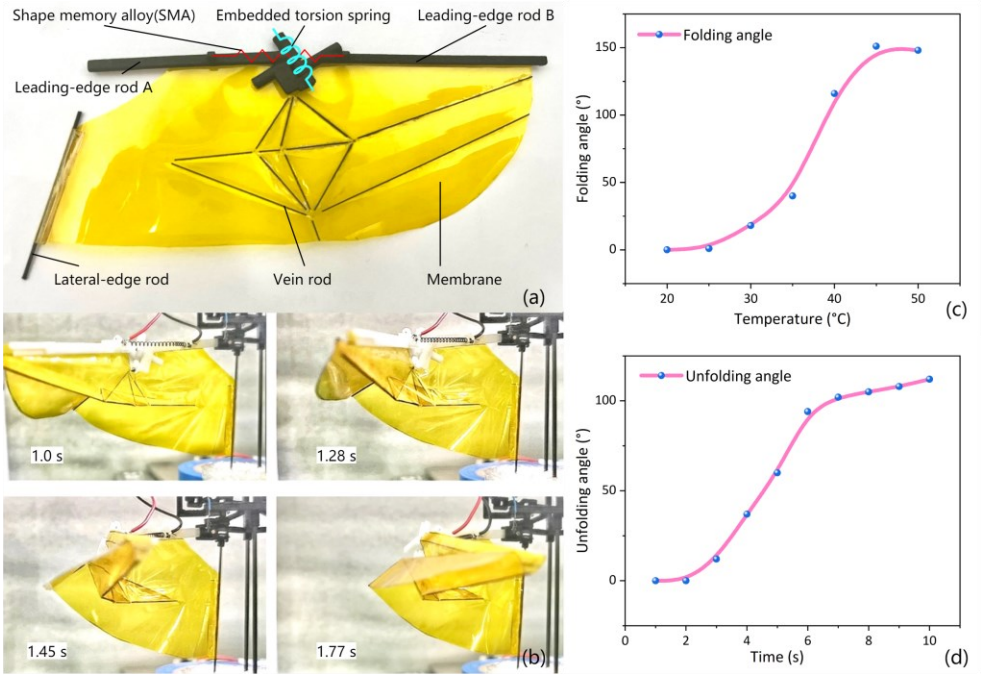

Fig. 6. Bionic foldable wing and folding test. (a) Prototyped foldable wing. (b) Folding process of the bionic wing. (c) The relationship between folding angle and temperature. (d) The relationship between unfolding angle and time.

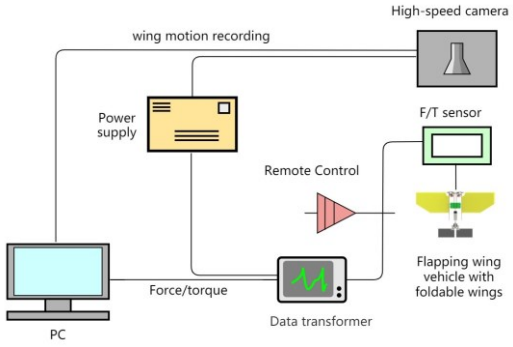

Fig. 7. Diagram of aerodynamic force/torque test system.

Table 1

Comparison of parameters between bionic foldable wings and hind wings of ladybird

Parameters	Bionic foldable wings	Hind wings of ladybird
unfolded wingspan	110 mm	9.75 mm
Folded wingspan	55 mm	4.67 mm
Fold angle (°)	142	160
Unfolded wing area	46.08 cm^2	17.33 mm^2
Folded wing area	23.31cm^2	6.19 mm^2
Weight (g)	1.1	<0.1
Folding ratio	2.0	2.8

folding process was completed within 1.8 s. The first second is the response process of the SMA spring. When the temperature increased gradually, the SMA spring began to contract at 1 s and returned to its original state in 1.77 s, completing the folding process. In terms of the folding effect, the diamond crease folded successfully according to the design trajectory. The relationship between the folding angle and the temperature is shown in Fig. 6(c). It can be observed that the SMA spring started responding at 25 ℃, and as the SMA spring responded rapidly from 35 ℃ to 45 ℃ , the folding angle increased substantially. The SMA spring produced the largest force and the folding process was completed in 1 s.

The unfolding of the foldable wing was completed within 10 s. When the wings are folded, the torsion spring stores energy. When the SMA spring was powered off, the torsion spring started to release energy, and the wings started to expand. The relationship between the unfolding angle and the time is shown in Fig. 6(d). It can be seen that the change in speed of the deployment angle in the initial three seconds was very slow. At this time, the SMA spring was powered off, and the temperature is slowly decreasing. The force of the torsion spring is not sufficient to pull the SMA spring; within 3 ~ 6 s, the torsion spring begins to release energy, and the wings gradually unfold. Within 6 ~ 10 s, the wing deployment slows

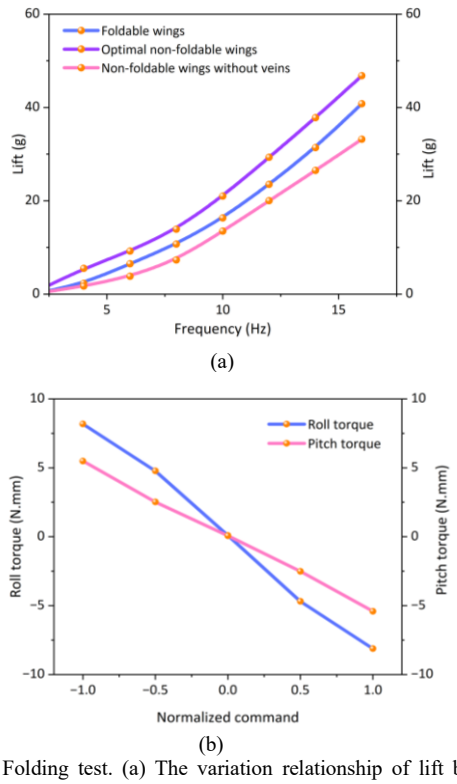

Fig. 8. Folding test. (a) The variation relationship of lift between foldable wing and flapping frequency. (b) Pitch and roll torques for various positions of the control actuators.

down owing to material limitations and the release of most of the energy by the torsion spring, which is in equilibrium with the SMA spring. Table 1 shows a comparison of the foldable wing and the hind wing parameters of ladybirds. Due to the fact that the muscles at the wing root of the ladybird can fully fit the wings with the body, this paper did not consider the folding motion at the wing root. Therefore, the folding ratio of ladybird is higher than that of current bionic foldable wings.

We built an aerodynamic/torque testing system to test the aerodynamic performance of the wings, as shown in Fig. 7. The platform was composed of a stabilised voltage supply, an iSpeed 716 high-speed cameras (iX Cameras, UK), an FWMAV prototype, an F6D45 sensor (ME, Germany), a GSV-8DS data signal amplifier, an ME software system, and a damping platform.

As shown in Fig. 8(a), when the flapping frequency was 14 Hz, the lift generated by the wings exceeded 34 g, whereas the total weight of the vehicle equipped with foldable wings was 33.6 g, which satisfied the flight aerodynamic conditions. When the remote control throttle reaches its maximum value, the total lift of the vehicle is close to 40 g. The attitude torque determines the maneuverability of an FWMAV. Fig. 8(b) shows the evolution of the pitch torque as a function of the position of the pitch actuator (normalised to its maximum), and it also shows the roll torque as a function of the normalised position of the roll actuator. The maximum pitch torque generated by the vehicle is 5.49 N.mm, and the maximum rolling torque is 8.18 N.mm. By comparing FWMAVs of the same size, the lift and attitude torques of the

Fig. 9. Flight test of FWMAV equipped with bionic foldable wings.

proposed vehicle meet the flight requirements. Fig. 9 shows the flight test of an FWMAV with bionic folding wings.

V. CONCLUSION

In this study, a bionic foldable wing based on ladybird's hindwing for FWMAV was presented. This paper analysed the crease and folding motion of the hind wing of the ladybird, combined the crease of the hind wing with the origami mechanism, a kinematic model of the folding mechanism based on the rigid origami mechanism is established, and a display expression for the unknown folding angle is derived to obtain the actual folding angle for any folding configuration. The real-time position coordinates of the vertices in any folded configuration are calculated using a rotation transformation matrix.

A combination of the SMA and torsion springs was used to simulate the tape spring structure of the hind wing of the ladybird, and the foldable wing prototype was manufactured and assembled. We conducted flight tests and aerodynamic experiments on an FWMAV equipped with foldable wings to verify its functionality and performance. During the flapping process, the SMA and torsion springs exhibited a slight torsional deformation, which may explain why the lift of the foldable wings was less than that of the non-foldable wings. However, the existing spring combination cannot match the tape spring structure of the hindwing of the ladybird. Future studies should focus on the performance of tape springs to improve the performance of foldable wings and flapping vehicles.

REFERENCES

[1] Haas F, Gorb S, Wootton RJ. Elastic joints in dermapteran hind wings: materials and wing folding. Arthropod Struc Dev 2000;29(2):137-146.

[2] Preumont A, Wang H, Kang S, Wang K, Roshanbin A. A Note on the Electromechanical Design of a Robotic Hummingbird. Actuators 2021,10, 52.

[3] Muhammad A, Park HC, Hwang DY, Byun D, Goo NS. Mimicking unfolding motion of a beetle hind wing. Chinese Science Bulletin 2009;54(14):2416-2424.

[4] Muhammad A, Nguyen QV, Park HC, Hwang DY, Byun D, Goo NS. Improvement of artificial foldable wing models by mimicking the unfolding/folding mechanism of a beetle hind wing. Journal of Bionic Engineering 2010;7(2):134-141.

[5] Truong QT, Argyoganendro BW, Park HC. Design and demonstration of insect mimicking foldable artificial wing using four-bar linkage systems. Journal of Bionic Engineering 2014;11(3):449-458.

[6] Stowers AK, Lentink D. Folding in and out: passive morphing in flapping wings. Bioinspiration & biomimetics 2015;10(2):025001.

[7] Ramezani A, Shi X, Chung SJ, Hutchinson S. Bat Bot (B2), a biologically inspired flying machine. 2016 IEEE International Conference on Robotics and Automation (ICRA) , Stockholm, Sweden; 2016. p. 3219-3226.

[8] Kovač M, Fauria O, Zufferey JC, Floreano D. The EPFL jumpglider: A hybrid jumping and gliding robot with rigid or folding wings. 2011 IEEE International Conference on Robotics and Biomimetics 2011.

[9] Guangping H, Nan M. Design and analysis of bat-like folding flapping wing mechanism. Journal of North China University of Technology 2014;26(3):35-41.

[10] Yongfeng W. Research on bionic foldable wing based on the hind wing of scarab. Jilin University 2016.

[11] Phan HV, Kang T, Park HC. Design and stable flight of a 21g insect-like tailless flapping wing micro air vehicle with angular rates feedback control. Bioinspiration & Biomimetics 2017;12(3):036006.

[12] Phan HV and Park HC. Design and evaluation of a deformable wing configuration for economical hovering flight of an insect-like tailless flying robot. Bioinspiration & Biomimetics 2018;13(3):036009.

[13] Sang-Min B, Sojung Y, Soo-Hwan C, Dae-Young L, Kyu-Jin C. Ladybird beetle–inspired compliant origami. Sci. Robot 2020;5:eaaz6262.

[14] Xiao S, Hu K, Huang B, Deng H, Ding X. A review of research on the mechanical design of hoverable flapping wing micro-air vehicles. Journal of Bionic Engineering 2021;18(6):1235-1254.

[15] Xiao S, Deng H, Hu K, Zhang S. Design and control of hoverable bionic flapping wing micro air vehicle. 2021 IEEE International conference on Electrical Engineering and Mechatronics Technology (ICEEMT), Qingdao, China; 2021. p. 224-227.

[16] Feng H, Peng R, Zang S, Ma J, Chen Y. Rigid foldability and mountain-valley crease assignments of square-twist origami pattern. Mechanism and Machine Theory 2020:103947.

[17] Kazuya S, Shuhei N, Shuhei Y, Ryuma N, Yoji O. Investigation of hindwing folding in ladybird beetles by artificial elytron transplantation and microcomputed tomography. Proc. Natl. Acad. Sci. 2017;114 (22):5624-5628.

[18] Zhang J, Zhao N, Qu F. Bio-inspired flapping wing robots with foldable or deformable wings: a review, Bioinspiration & Biomimetics 2022;Nov:18(1).

[19] Chen Z, Chen Q, Jia G, Dai J. Sylvester's dialytic elimination in analysis of a metamorphic mechanism derived from ladybird wings. Mechanism and Machine Theory 2023; 179.

[20] Yu H, Guo Z, Wang J. A method of calculating the degree of freedom of foldable plate rigid origami with adjacency matrix. Advances in Mechanical Engineering 2018;10(6):168781401877969.

[21] Dai JS, Huang Z, Lipkin H. Mobility of overconstrained parallel mechanisms. Asme J.mech.des 2006;128(1):220-229.

[22] Huang Z, Li Q, Ding H. Theory of parallel mechanisms. Mech Mach Sci 2012;6: 653–654.

[23] Chen X, Feng H, Ma J, Chen Y. A plane linkage and its tessellation for deployable structure. Mechanism and Machine Theory 2019;142:103605.

[24] Jaronie Mohd Jani, Martin Leary, Aleksandar Subic, et al. A review of shape memory alloy research, applications and opportunities. Materials and Design. 2014;56:1078–1113.